Rev.Adv.Mater.Sci. 18(2008) 469-475

CRYSTALLIZATION BEHAVIOR OF AMORPHOUS ALLOYS IN THE Al-Ce-Ni SYSTEM

C. Triveño Rios[1], S. Suriñach[2], M. D. Baró[2], C. Bolfarini[1], W. J. Botta F.[1] and C. S. Kiminami[1]

[1]Department of Materials Engineering, Federal University of São Carlos, SP, Brazil
[2]Department of Physics, Autonomous University of Barcelona, Bellaterra, Barcelona, Spain

Received: March 29, 2009

Abstract. This work involved an investigation of the crystallization process of $Al_{90}Ce_5Ni_5$ amorphous alloy. Rapidly quenched amorphous ribbon was produced by melt-spinning and the structural transformations occurring during heating were studied using a combination of X-ray diffraction (XRD) and differential scanning calorimetry (DSC). Crystallization took place through a multistage process. The first stage of transformation corresponded to the crystallization of the fcc-Al phase, while the second and third exothermic transformations involved the crystallization of Al_3Ni, $Al_{11}Ce_3$, Al_3Ce, AlCeNi and unidentified phases. The transformation curves recorded under isothermal treatments at 150 °C and 305 °C indicated that crystallization occurred through nucleation and growth, with diffusion-controlled growth occurring in the first crystallization stage and interface-controlled growth in the third. The Avrami exponents suggested only crystallization of fcc-Al phase, and simultaneous crystallization of intermetallic compounds and unidentified phases with two- and three-dimensional crystallization.

1. INTRODUCTION

Since 1984, much attention has focused on Al–rare earth (RE) alloys, particularly because of the relatively high glass forming ability of some compositions and their special properties, which make them suitable for high temperature applications [1]. Aluminum-based metallic glasses with high Al content in compositional ranges above 80 at.% Al, combined with transition metal (TM) and rare earth (RE) [2] i.e., Al-TM(Fe, Co, Ni)-RE(La, Y, Ce) [2-4], have been studied intensively due to their mechanical properties, including tensile strength as high as 1000 MPa, which is about double that of conventional high-strength aluminum alloys. The mechanical properties have been further improved by partial crystallization of the amorphous structure, forming a homogeneous precipitation of nanometer-sized fcc-Al phase in the amorphous matrix [5]. The mechanical properties of these nano-amorphous composite materials have attracted increased interest for their potential industrial applications and as subjects to gain a fundamental understanding of the special structure-property relationship of this new class of materials. In this paper, we report on the crystallization behavior upon annealing of amorphous $Al_{90}Ce_5Ni_5$ melt-spun ribbons, analyzed with a combination of DSC and XRD.

2. EXPERIMENTAL DETAILS

$Al_{90}Ce_5Ni_5$ alloy was prepared by arc melting of high-purity Al, Ni, and Ce in an argon atmosphere. Amorphous ribbon was produced by a single-roller melt-spinning technique under argon with a Cu–wheel rotating at a velocity of ~54 $m.s^{-1}$. The 2-3 mm wide, 30-40 μm thick as-quenched ribbon presented a bending ductility of 180°. The amorphous as-quenched and partially crystallized samples were

Corresponding author: Walter Jose Botta, e-mail: cbolfa@power.ufscar.br

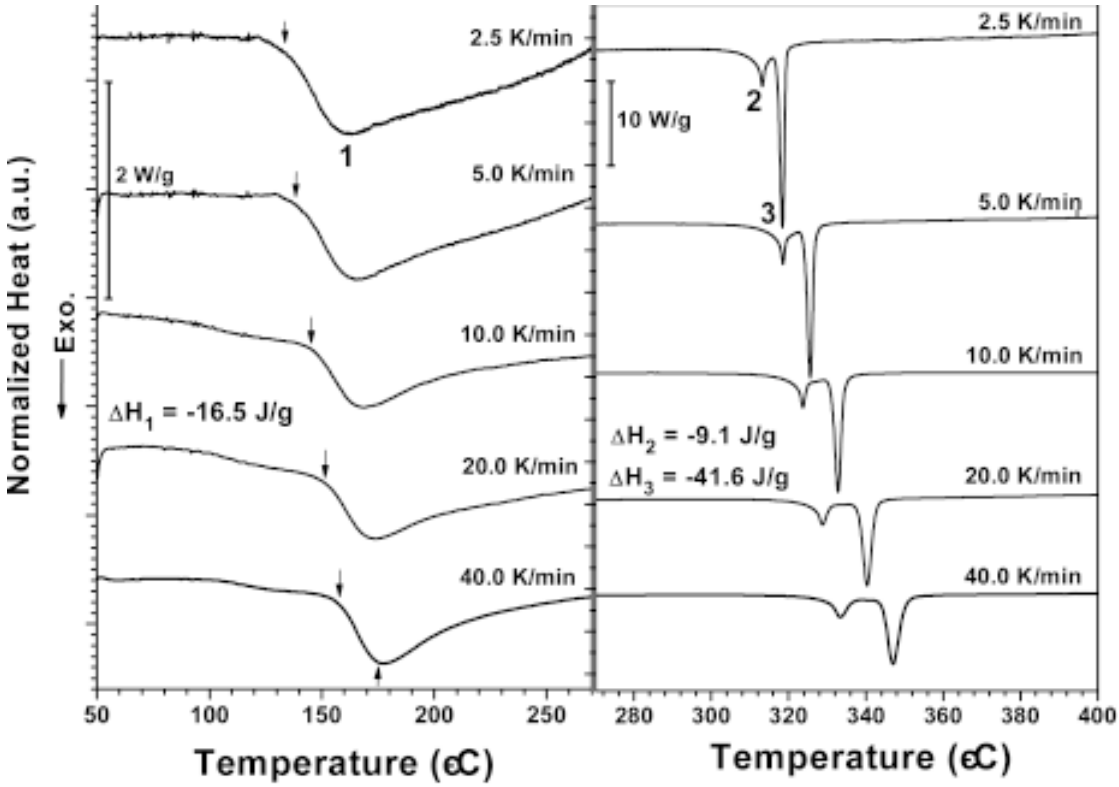

Fig. 1. DSC-curves obtained at different continuous heating rates: (a) first crystallization peak, and (b) second and third crystallization peaks.

examined by X-ray diffraction (XRD) using CuK_α, and by transmission electron microscopy (TEM). Thermal analyses were performed in a Perkin–Elmer DSC-7 calorimeter. Continuous heating studies were carried out in a heating range and rate of 2.5-40 K/min. Isothermal treatments consisted of continuous heating at a rate of 100 K/min up to the treatment temperature.

3. RESULTS AND DISCUSSION

Figs. 1a and 1b present the normalized thermograms of as-quenched amorphous ribbon heated at different rates (β = 2.5-40 K/min). Fig. 1a shows the first crystallization peak when fcc-Al was formed. Fig. 1b shows the second and third crystallization peaks when intermetallic compounds, metastable phase and additional fcc-Al phases were formed. As can be seen, increasing the heating rate caused all the crystallization peaks to shift to higher temperatures. Congruous with a previous study [6], the absence of T_g indicated that in the entire Al-Ce-Ni system, the glass transition phenomenon occurred only in the composition with Ce content above 6.0 at.% and was independent of the Ni content.

The activation energy for crystallization of the amorphous structure can be estimated under a continuous heating condition, using Kissinger's model [7]. Fig. 2 shows that the Kissinger plot $R\times\ln(\beta/T_p)$ versus $(1/T_p)$ yields straight lines with a good fit. From the slope of the line, the activation energy (E_a) can be estimated for the crystallization stages. Here, β is the heating rate, T_p the crystallization temperature peaks, and R is the universal gas constant. An evaluation of the activation energies for the crystallization of each peak indicated that the activation energy for the first peak of crystallization, where fcc-Al phase forms, was approximately 250 kJ/mol. This value, although lower than those of the other peaks, was higher than that of inter-diffusion in pure Al (~145 kJ/mol) [8], suggest-

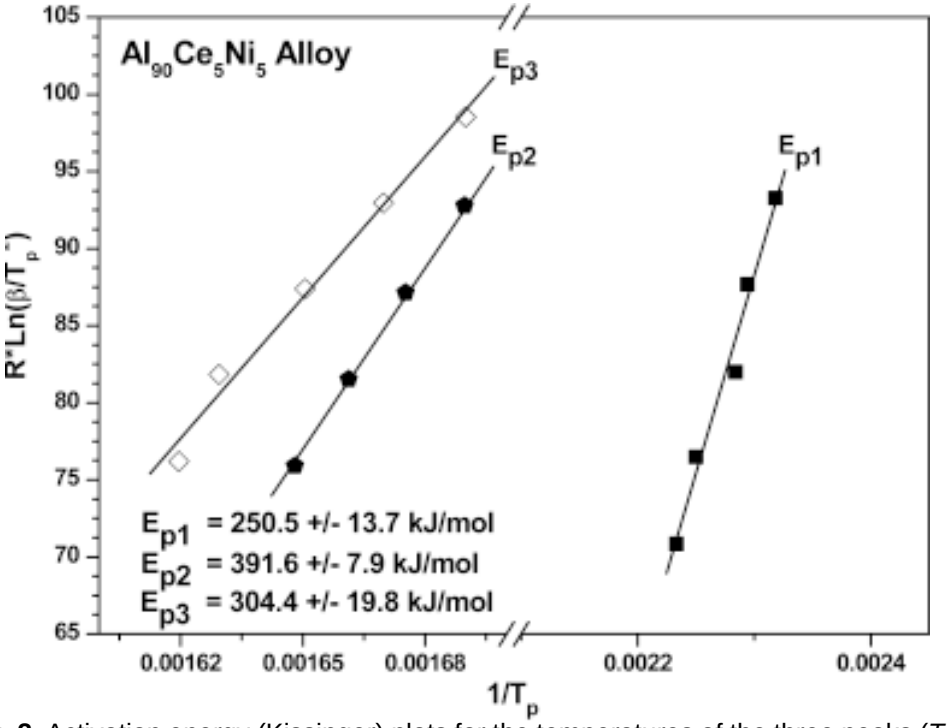

Fig. 2. Activation energy (Kissinger) plots for the temperatures of the three peaks (T_p).

ing that diffusion of the solute elements (Ni and Ce) is involved in this nanocrystallization process, in which the solutes are completely ejected from the crystallites into the amorphous matrix [9]. The higher values of the activation energy of the second and third crystallization peaks, ~391.6 and 304.4 kJ/mol, respectively, corresponded to the formation of residual fcc-Al and polyphase crystallization. The higher values of the activation energies suggest a higher thermal stability of the corresponding phases than that of the fcc-Al phase.

Fig. 3 presents the XRD patterns of the as-quenched and annealed ribbons. The heat treatment was applied at 150 °C for 30 min, corresponding to the first crystallization peak. The XRD patterns indicate amorphous structure for the as-quenched ribbon and formation of fcc-Al phase by crystallization in the first stage. The considerable enlargement of the fcc-Al peaks indicates that a small amount of either Ni or Ce was retained in solid solution in the Al phase. However, the average crystalline size, estimated by the Scherrer formula [10] with full width at half maximum of the (111) fcc-Al diffraction peak, was smaller than 10 nm. This size estimation is congruent with the value of 10 nm for the first hour of annealing at 150 °C reported previously for $Al_{90}Ce_4Ni_6$ alloy [11]. The inset in Fig. 3 shows a thermogram obtained in isothermal mode for the as-quenched ribbon at 150 °C. A monotonically decreasing exothermic DSC signal typical of grain growth [12] was not observed. However, a bell-shaped DSC signal, which was not well defined in the initial stage, indicated that the crystallization transformation occurred by an fcc-Al nucleation/growth process. The fact that the isothermal thermoanalysis indicated that released was lower (-16.5 J/g) than that released during isochronic heating corroborates the mechanism of grain nucleation and growth. Asymmetric isothermal thermograms such as the one shown in the inset in Fig. 3 are usually [13] related to diffusion-controlled growth in alloys with primary crystallization.

Fig. 4 presents XRD patterns for the as-quenched and annealed ribbons. The heat treatment was applied for different lengths of time at 305 °C, corresponding to the second and third crystallization peaks. The inset in Fig. 4 shows a thermogram in the isothermal mode of the as-quenched ribbon at 305 °C. The thermogram shows two exothermic reactions, indicating the occurrence of two

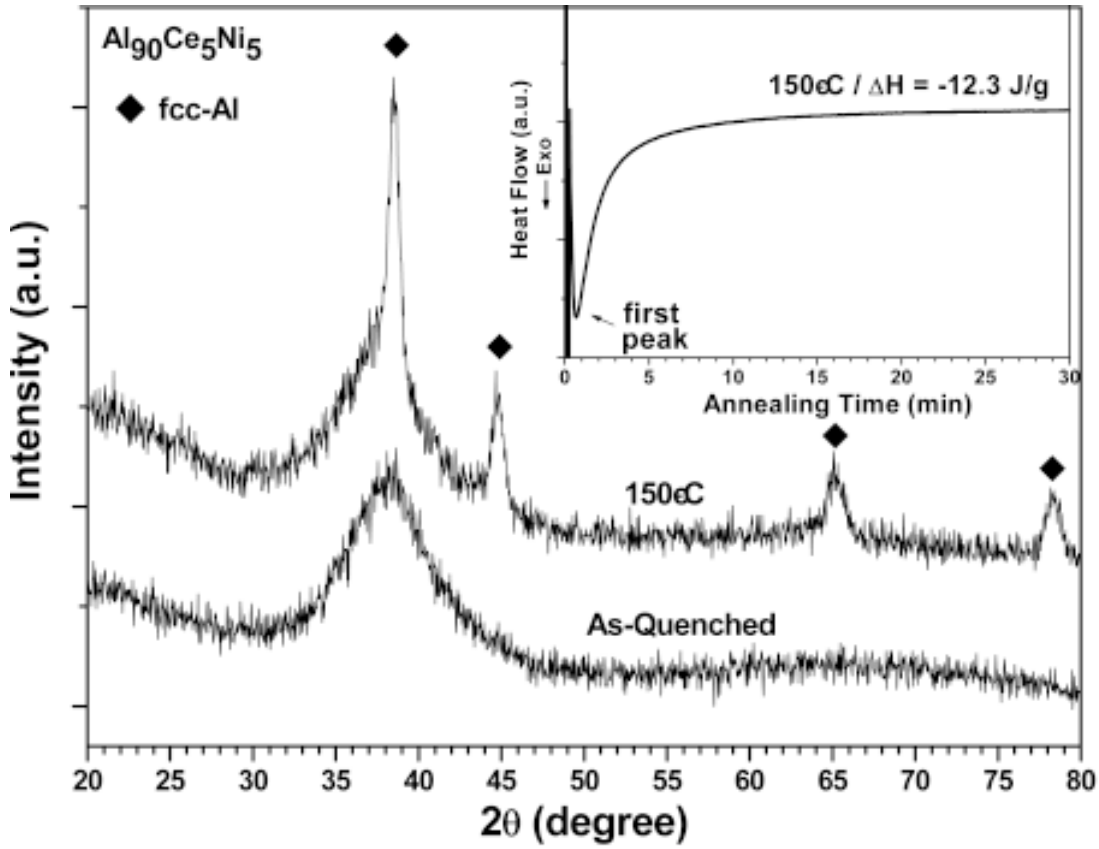

Fig. 3. XRD patterns of the as-quenched and annealed ribbon. The heat treatment was applied at 150 °C for 30 min, corresponding to the first crystallization peak. The inset shows a thermogram of the as-quenched ribbon isothermally treated at 150 °C.

clearly distinguishable crystallization stages. The XRD patterns indicate formation of fcc-Al phase for treatment times varying from 5 to 12 min. The average crystallite size estimated by the Scherrer formula [10] from (111) fcc-Al peak was smaller than 15bnm.

After longer treatment times (> 12 min. for second crystallization, inset in Fig. 4), the XRD patterns reveal low intensity, broad diffraction peaks corresponding to the first traces of Al_3Ni, Al_3Ce, $Al_{11}Ce_3$, and AlCeNi intermetallic compounds and unidentified phases precipitated from the residual amorphous matrix. The isothermal thermogram indicates that this second crystallization stage involved a small amount of released (about -11.4 J/g) similar to that occurring in second stage crystallization under continuous heating (about -9.1 J/g), suggesting that this stage is governed by the nucleation/growth mechanism characteristic of intermetallic compounds. The slightly larger amount of heat released, in this case, may have been due to the nucleation activation energy of the intermetallic compounds, to which the contribution of nucleation activation energy is much smaller than growth activation energy [14].

After even longer treatment times (16 min and 20 min at the third crystallization stage), the XRD patterns show the formation of a larger volume fraction of fcc-Al and unidentified intermetallic compounds. Therefore, this crystallization stage was governed mainly by the growth mechanism of unidentified, fcc-Al and intermetallic crystallites. The nucleatiion of new crystallites from the residual amorphous phase it is small amount and completed within a very short period of time. This behavior was confirmed by the isothermal thermogram (inset in Fig. 4), which shows a well defined bell-shaped DSC signal for the third crystallization stage, which is typical of a nucleation/growth mechanism, and by the slightly higher heat released

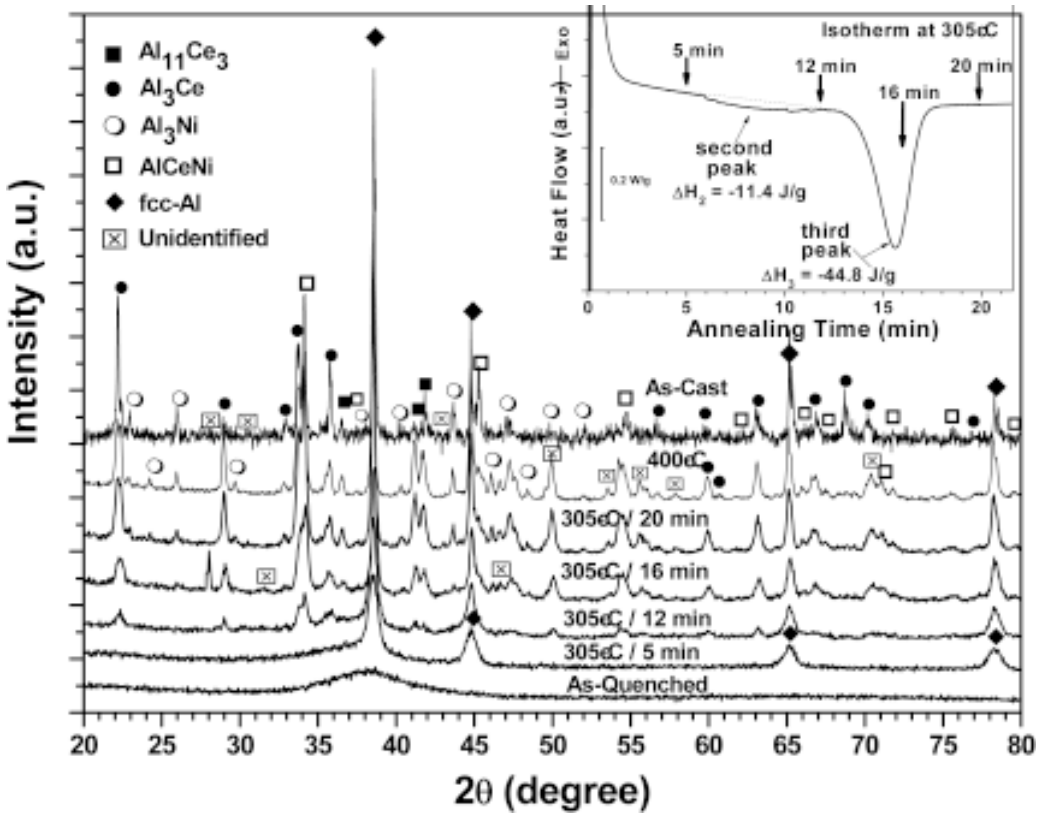

Fig. 4. XRD patterns of the as-quenched and annealed ribbon. The heat treatments were applied for different times at 305 °C, corresponding to the second and third crystallization peaks, for the crystallized ribbon at 400 °C and for the as-cast ingot cooled in conditions close to equilibrium. The inset in figure shows a thermogram of the as-quenched ribbon isothermally treated at 305 °C.

in those transformations (-44.8 J/g) than that released during continuous heating (-41.6 J/g).

Fig. 4 also presents XRD patterns for the fully crystalline ingot (cooled close to equilibrium) and for the annealed ribbon. The heat treatment was applied by continuous heating at 20 K/min up to 400 °C, which may have led to full crystallization, according to the thermogram in Fig. 1b. The crystallized ribbon showed a larger amount of crystallization of the unidentified phase, fcc-Al and intermetallic compounds. By comparison with the patterns of the ingot, the ones corresponding to the $Al_{11}Ce_3$ and unidentified phases were not observed. The instability of the metastable $Al_{11}Ce_3$ phase above 460 °C, with a stable microstructure composed of fcc-Al, hexagonal Al_3Ce and orthorhombic Al_3Ni, as well as some unidentified phases, have been reported in the literature [15] for $Al_{85}Ce_5Ni_8Co_2$ alloy, which is in agreement with our observations in this study.

An alternative method to study the isothermal crystallization kinetics is through the JMA model [16], known by the Avrami equation: $x = 1 - \exp[-(Kt)^n]$, where K is a constant, x is the crystalline fraction, and n is the Avrami exponent reflecting the mechanism of nucleation and growth during the phase transformation. The value of "n" for steady-state mechanisms, over the range of 15 to 85% of transformed fractions [18], can be calculated from the slope of the straight line of the $\ln[\ln(1/(1-x(t)))]$ vs. $\ln(t)$ plot. The JMA plots in this study did not show a linear relationship, implying that multiple mechanisms may have been involved in the amorphous-to-crystalline transformation. The Avrami exponent, n, was 1.8±0.3 in the first crystallization process. This value suggests that the

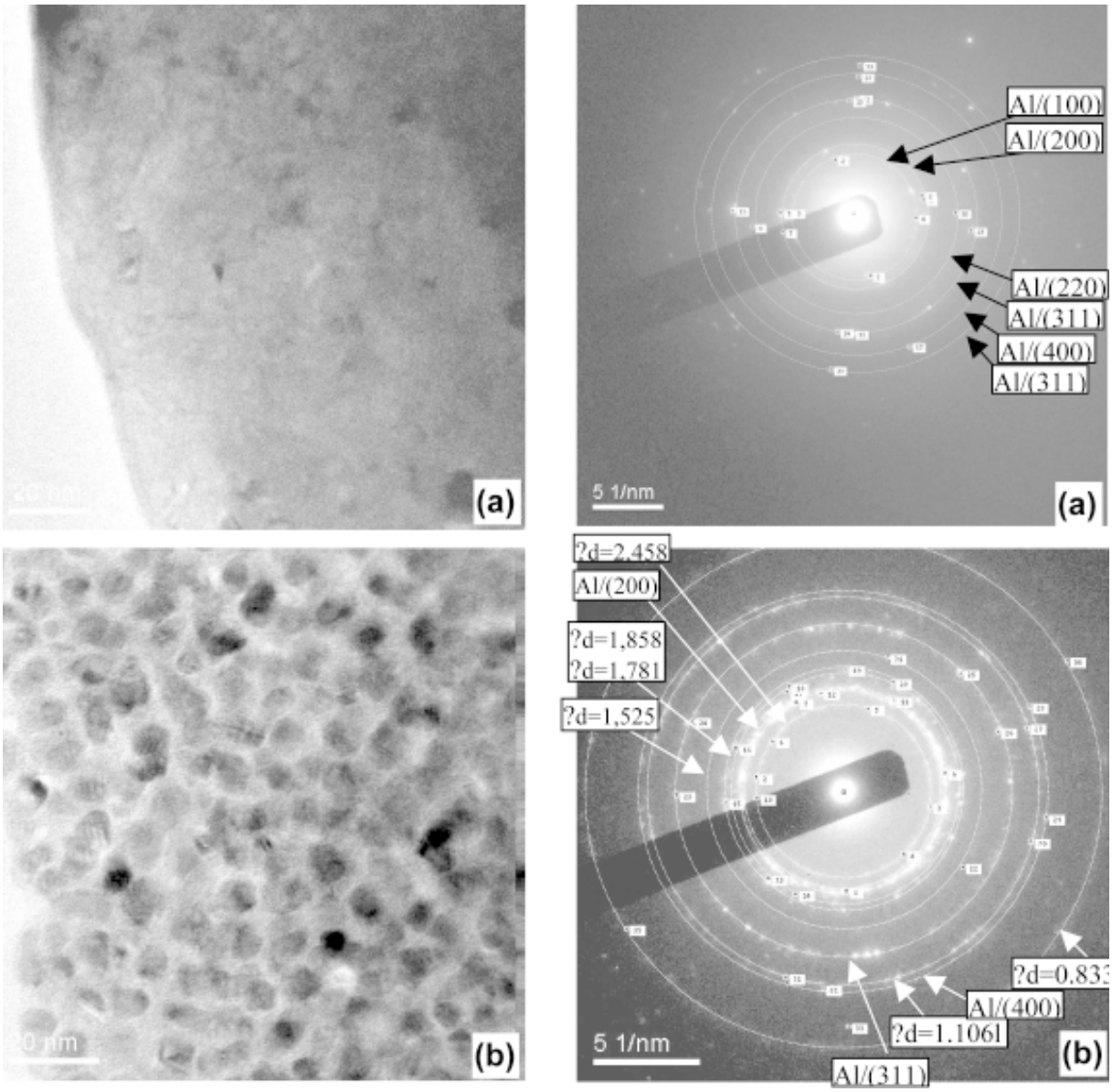

Fig. 5. Dark field TEM-images and corresponding selected-area electron diffraction patterns of ribbons after isothermal annealing at: (a) 150 °C for 30 min, and (b) 305 °C for 16 min.

transformation in the intermediate stage was governed by two-dimensional diffusion-controlled growth with instantaneous nucleation [18]. This behavior agrees well with the shape of the asymmetric isothermal curve shown in the inset of Fig. 4. However, the Avrami exponent, n, for the third crystallization process was 3.4±0.5, suggesting that the transformation in the intermediate stage was governed by three-dimensional interface-controlled growth with homogeneous nucleation at a constant rate [18], which is also congruous with the shape of the symmetric isothermal curve in the inset of Fig. 4.

The formation of fcc-Al nanocrystals indicated by the XRD pattern of the ribbon annealed at 150 °C for 30 min (Fig. 3) was confirmed by a microstructural examination using dark field TEM (Fig. 5a). The microstructure consisted solely of randomly distributed fcc-Al nanocrystals with sizes of about 10 nm embedded in the amorphous phase. Also, the formation of fcc-Al, intermetallic compounds and some unidentified phases, which was

indicated by the XRD pattern of the annealed at 305 °C for 16 min (Fig. 5b), was confirmed by TEM, which revealed spherical-shaped nanocrystals about 15±5 nm in size embedded in the residual amorphous phase located between the crystallized grains. The crystallized amorphous fraction corresponded to 76±6% in an average of eight pictures. In this case, the respective diffraction rings revealed the presence of fcc-Al and unidentified phases. The unidentified phases showed interplanar distances unlike those of the fcc-Al phase.

4. CONCLUSIONS

The crystallization of the amorphous $Al_{90}Ce_5Ni_5$ ribbon occurred through a multistage process. The first stage of transformation corresponded to the crystallization of the fcc-Al phase, while the second and third exothermic transformations corresponded to the crystallization of Al_3Ni, $Al_{11}Ce_3$, Al_3Ce, AlCeNi and unidentified phases. The isothermal treatments and the JMA analysis of the transformation curves measured at annealing temperatures of 150 °C and 305 °C indicated that crystallization occurred through nucleation and growth, with diffusion-controlled and interface-controlled growth in the first and third crystallization processes, respectively. The Avrami exponents for the first and third crystallization processes were 1.8±0.3 and 3.4±0.3, respectively, suggesting only crystallization of fcc-Al phase and simultaneous crystallization of intermetallic compounds and unidentified phases with two- and three-dimensional crystallization, respectively.

ACKNOWLEDGEMENTS

The authors gratefully acknowledge the financial support of FAPESP and CNPq (Brazil), and of Materials II Physics Group of the Department of Physics – Autonomous University of Barcelona (Spain).

REFERENCES

[1] M. Fass, D. Itzhak, D. Eliezer and F.H. Froes // *J. Mater. Sci. Lett*. **6** (1987) 1227.
[2] A. Inoue, K. Ohtera, A.P. Tsai and T. Masumoto // *Jpn. J. Appl. Phys*. **27** (1988) L479.
[3] Y.H. Kim, A. Inoue and T. Masumoto // *Mater. Trans. JIM* **32** (1991) 331.
[4] T. Gloriant and A. L. Greer // *Nanostruct. Mater.* **10** (1998) 389.
[5] H. Chen, Y. He, G.J. Shiet and S. J. Poon // Scripta Metall. **225** (1991) 1421.
[6] A. Inoue, K. Ohtera, A. P. Tsai, H. Kimura and T. Masumoto // *Jpn. J. Appl. Phys*. **27** (1988) L1579.
[7] H. E. Kissinger // *Analyt. Chem.* **29** (1957) 1702.
[8] M. Gich, T. Gloriant, S. Suriñach, A. L. Greer and M. D. Baró // *J. Non-Cryst. Solids* **289** (2001) 214.
[9] J. C. Foley, D. R. Allen and J. H. Perepezko // *Mater. Sci. Eng. A* **226-228** (1997) 569.
[10] H. P. Klug and L. E. Alexander, *X-ray Diffraction Procedures for Polycristalline an Amorphous Materials* (Wiley, N.Y., 1974).
[11] M. A. Muñoz-Morris, S. Suriñach, M. Gich, M. D. Baró and D. G. Morris // *Acta Mater* **51** (2003) 1067.
[12] L. C. Chen and F. Saepen // *Nature* **336** (1988) 366.
[13] T. Pradell, D Crespo, N Clavaguera and M. T. Clavaguera-Mora // *J. Phys.: Condens. Matter* **10** (1998) 3833.
[14] F. Ye and K. Lu // *Journal of Non-Crystalline Solids* **262** (2000) 228.
[15] Á. Révész, G. Heunen, L. K. Varga, S. Suriñach and M. D. Baró // *J. Alloys Comp.* **368** (2004) 164.
[16] M. Avrami // *J. Phys. Chem.* **8** (1940) 212.
[17] L. Liu and K.C. Chan // *J. Alloys Comp.* **364** (2004) 146.
[18] The theory of transformations in metals and alloys, ed. by J. W. Christian (Pergamon, London, 1981).